


## Article

# Dynamic Sliding Mode Control of DC-DC Converter to Extract the Maximum Power of Photovoltaic System Using Dual Sliding Observer

Ali Karami-Mollaei<sup>1</sup> and Oscar Barambones<sup>2,\*</sup> <sup>1</sup> Faculty of Electrical and Computer Engineering, Hakim Sabzevari University, Sabzevar 9617976487, Iran<sup>2</sup> Automatic Control and System Engineering Department, University of the Basque Country, UPV/EHU, Nieves Cano 12, 01006 Vitoria-Gasteiz, Spain

\* Correspondence: oscar.barambones@ehu.eus; Tel.: +34-94-501-3235; Fax: +34-94-501-3270

**Abstract:** This paper concerns the maximum power extraction of a photovoltaic generator system (PGS). The PGS consists of single photovoltaic (PV) cells. To improve the efficiency of a PGS, it is necessary to work within its maximum power point (MPP). In a PGS, output power is dependent on solar irradiance and the operating temperature and, therefore, MPP would be varied. To address this problem, a converter should be placed after the PGS and a smooth control signal should be used to adjust its duty cycle. The other challenge of a total system, i.e., PGS and converter, is the uncertainty involved. To overcome this uncertainty, a dynamic sliding mode control (SMC) can be used to regulate the smooth duty cycle. The low-pass integrator before the system can remove the chattering in dynamic SMC. However, due to the integrator, the states of the system increase and, hence, we propose a dual sliding observer (DSO) to estimate this added state. For a reliable comparison with the conventional SMC, the same proposed DSO can be applied in both dynamic and conventional SMC. The provided comparison shows the effectiveness of dynamic SMC in chattering suppression and real implementation with respect to conventional SMC.

**Keywords:** photovoltaic generator system; converter control; dual sliding observer; sliding mode control



**Citation:** Karami-Mollaei, A.; Barambones, O. Dynamic Sliding Mode Control of DC-DC Converter to Extract the Maximum Power of Photovoltaic System Using Dual Sliding Observer. *Electronics* **2022**, *11*, 2506. <https://doi.org/10.3390/electronics11162506>

Academic Editors: Juan Rodríguez Méndez and Aitor Vázquez Ardura

Received: 15 July 2022

Accepted: 8 August 2022

Published: 11 August 2022

**Publisher's Note:** MDPI stays neutral with regard to jurisdictional claims in published maps and institutional affiliations.



**Copyright:** © 2022 by the authors. Licensee MDPI, Basel, Switzerland. This article is an open access article distributed under the terms and conditions of the Creative Commons Attribution (CC BY) license (<https://creativecommons.org/licenses/by/4.0/>).

## 1. Introduction

The increase in the consumption of fossil fuels has been shown to result in global warming. This can be prevented by more widespread use of wind and solar energy [1–3], which are clean, renewable, and accessible [4]. Solar energy in particular has attracted much attention because of economical use of a photovoltaic generator system (PGS) on a worldwide scale [5]. Nevertheless, the output power of PGS is dependent on temperature and on solar irradiation [6]. Hence, to improve the efficiency of a PGS, it is necessary to extract its maximum power by a maximum power point tracking (MPPT) controller [7]. It has been shown that MPPT can be achieved using a DC-DC power converter after the PGS and adjusting its duty cycle [6,7]. Many MPPT controllers have been proposed in the literature [8–11]. Some approaches are based on a neural network [8] or on the fuzzy method [9,10]. The P&O methods oscillate around the MPPT [11].

Due to the overall uncertainty associated with these systems, a robust controller such as sliding mode control (SMC) is needed to regulate the duty cycle. SMC is invariant, which is its most important property and is stronger than its robustness [12–14]. For this reason, SMC is used in many MPPT controllers [15–22]. In most of these works, however, SMC suffers from chattering as a disadvantage phenomenon; this is due to the use of sign function [12–14], as a result of which a smooth duty cycle cannot be produced. (Note that the duty cycle should be a smooth signal between zero and one.)

To remove chattering, some methodologies are proposed in the literature [23]: boundary layer SMC [24], adaptive boundary layer SMC [25–27], higher order SMC [28,29], and dynamic SMC [30,31]. In boundary layer SMC and adaptive boundary layer SMC, the invariance, as the predominant property of SMC, is missed [23]. Higher-order SMC requires the higher-order derivatives of the system function, which should be estimated using an observer [32–36]. However, in dynamic SMC, the effect of discontinuous sign function is suppressed by a low-pass integrator, which is located before the system model [31]. Then the system states increase due to the dynamic behavior of this integrator. Therefore, this augmented state should be estimated using an observer. Whereas in higher-order SMC the differentiation of the system model should be estimated, in dynamic SMC the increased state should be estimated; this constitutes the priority of dynamic SMC.

Moreover, the concepts of model identification [37,38], parameters identification [39,40], and disturbance observer [41] are used for the control of linear and nonlinear systems, which also use known inputs and outputs of systems as feedback. Furthermore, similar to the SMC, sliding observers have invariance property against uncertainty and disturbance [42,43].

Motivated by the above discussion, chattering is the most critical of all these factors. Therefore, based on the disadvantages problem of boundary layer SMC, adaptive boundary layer SMC, and higher-order SMC, we propose a dynamic SMC method for the MPPT control of PGS to reliably prevent chattering while preserving the invariance property to overcome the inherent uncertainty of the model. Moreover, to implement this controller and to identify the plant model, a new dual sliding observer (DSO) is constructed. Thereafter, the theory of Lyapunov stability is used for the stabilization proof of dynamic SMC and DSO.

Therefore, the proposed structure is preceded in six sections. At first, the PGS model description is presented in Section 2. Then problem formulation and proposed dual observer design are discussed in Section 3. Finally, in Sections 5 and 6, simulation results and a conclusion are provided, respectively.

## 2. Model Description

The system consists of a PGS and a DC-DC converter [19], as in Figure 1.

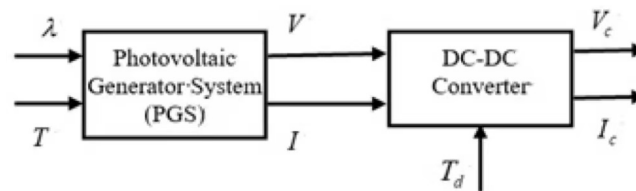


Figure 1. The overall model.

Where  $\lambda$  is solar irradiation,  $T$  is cell temperature,  $V$  and  $I$  are PGS voltage and current outputs,  $T_d$  is the duty cycle of converter, and  $V_c$  and  $I_c$  are the fixed outputs voltage and current of converter.

### 2.1. Photovoltaic Generator System (PGS) Model

A single PV cell is shown in Figure 2 and its output current is described by the following equation [8–11,15–22]

$$I_{PV} = I_{ph} - I_D - I_{sh} \tag{1}$$

such that  $I_D$ ,  $I_{sh}$ , and  $I_{ph}$  are the diode current, shunt current, and current generated by the incident light, respectively; all of which can be described using the following equations.

$$I_D = I_r \left[ \exp \left( \frac{V_{PV} + R_s I_{PV}}{V_T} \right) - 1 \right] \tag{2}$$

$$I_{sh} = \frac{V_{PV} + R_s I_{PV}}{R_{sh}} \tag{3}$$

$$I_{ph} = [I_{sc} + K_I(T - T_r)] \frac{\lambda}{1000} \tag{4}$$

in which  $V_{PV}$  and  $I_{PV}$  are the voltage and current of this single PV,  $V_T = \frac{kT}{q}$  is the thermal voltage,  $T_r$  is the cell reference temperature,  $I_{sc}$  and  $K_I$  are the short-circuit current and temperature coefficient in the short-circuit case both at reference condition, and  $I_r$  is the cell reverse saturation current. Moreover,  $q$  is the electron charge ( $1.60217 \times 10^{-19}C$ ) and  $k$  is the Boltzmann's constant ( $1.38 \times 10^{-23}J/K$ ). As regards PGS, the relation between its output voltage and current, i.e.,  $V$  and  $I$  is as follows:

$$I = I_{phg} - I_{rg} \left[ \exp\left(\frac{V + R_{sg}I}{V_{Tg}}\right) - 1 \right] - \frac{V + R_{sg}I}{R_{shg}} \tag{5}$$

where  $R_{sg} = \frac{N_s}{N_p} R_s$ ,  $R_{shg} = \frac{N_s}{N_p} R_{sh}$ ,  $I_{phg} = N_p I_{ph}$ ,  $I_{rg} = N_p I_r$ ,  $V_{Tg} = \frac{N_s}{N_p} V_T$ , and  $N_s$  and  $N_p$  are the numbers of connected-series and parallel PV cells, respectively.

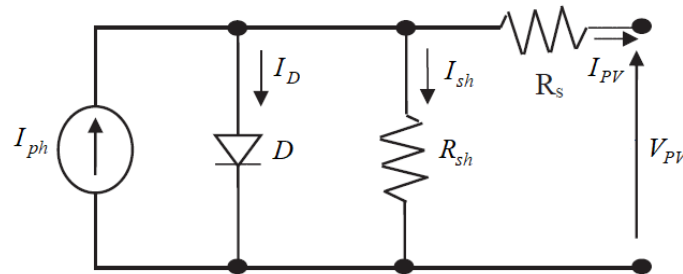


Figure 2. A single PV cell.

2.2. DC-DC Converter Model

The structure of the utilized converter in continuous conduction mode (CCM) is shown in Figure 3 and is described by the following equations.

$$C_i \frac{dV}{dt} = I - I_{Li} \tag{6}$$

$$L_i \frac{dI_{Li}}{dt} = V - (1 - T_d)V_c \tag{7}$$

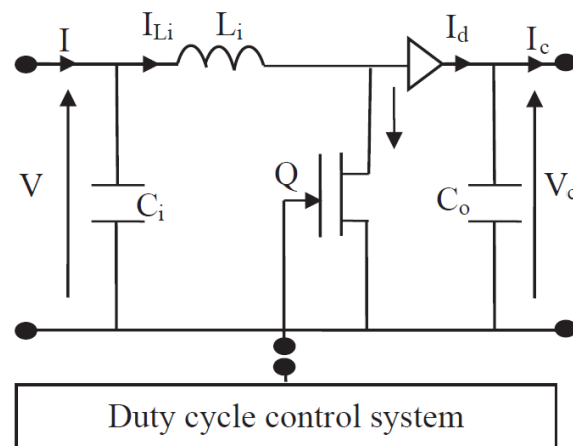


Figure 3. The DC-DC converter.

$I_{Li}$ ,  $L_i$ ,  $C_i$ , and  $C_o$  are, respectively, the current of inductor, the self-inductor, the input capacitor, and the output capacitor;  $Q$  is the semiconductor switch.

### 3. Problem Formulation and Observer Design

Using the two first sentences of Taylor series in Exponential function Equation (5), it follows that:

$$I = I_{phg} - I_{rg} \left( \frac{V + R_{sg}I}{V_{Tg}} \right) - \frac{V + R_{sg}I}{R_{shg}} \tag{8}$$

Rewritten, this results in the following algebraic equation:

$$\left( 1 + \frac{I_{rg}R_{sg}}{V_{Tg}} + \frac{R_{sg}}{R_{shg}} \right) I + \left( \frac{I_{rg}}{V_{Tg}} + \frac{1}{R_{shg}} \right) V = I_{phg} \tag{9}$$

Therefore, using Equation (6) into the second derivative of Equation (9) leads to:

$$\left( 1 + \frac{I_{rg}R_{sg}}{V_{Tg}} + \frac{R_{sg}}{R_{shg}} \right) \ddot{I} + \left( \frac{I_{rg}}{V_{Tg}} + \frac{1}{R_{shg}} \right) \left( \frac{\dot{I} - \dot{I}_{Li}}{C_i} \right) = \ddot{I}_{phg} \tag{10}$$

Rearranging this equation and using Equation (7) has the following result:

$$\left( 1 + \frac{I_{rg}R_{sg}}{V_{Tg}} + \frac{R_{sg}}{R_{shg}} \right) \ddot{I} + \frac{1}{C_i} \left( \frac{I_{rg}}{V_{Tg}} + \frac{1}{R_{shg}} \right) \dot{I} - \frac{1}{C_i} \left( \frac{I_{rg}}{V_{Tg}} + \frac{1}{R_{shg}} \right) \left( \frac{V + u}{L_i} \right) = \ddot{I}_{phg} \tag{11}$$

in which  $u = (T_d - 1)V_c$  is the input control signal of the system. Replacing variable  $V$  from Equation (9), it follows that:

$$\begin{aligned} &\left( 1 + \frac{I_{rg}R_{sg}}{V_{Tg}} + \frac{R_{sg}}{R_{shg}} \right) \ddot{I} + \frac{1}{C_i} \left( \frac{I_{rg}}{V_{Tg}} + \frac{1}{R_{shg}} \right) \dot{I} + \frac{1}{L_i C_i} \left( 1 + \frac{I_{rg}R_{sg}}{V_{Tg}} + \frac{R_{sg}}{R_{shg}} \right) I \\ &- \frac{1}{L_i C_i} \left( \frac{I_{rg}}{V_{Tg}} + \frac{1}{R_{shg}} \right) u = \frac{1}{L_i C_i} \left( \frac{I_{rg}}{V_{Tg}} + \frac{1}{R_{shg}} \right) I_{phg} + \ddot{I}_{phg} \end{aligned} \tag{12}$$

Using the definition of  $x_1 = I$  and  $x_2 = \dot{I}$ , the matrix form of the last equation is as:

$$\dot{x} = Ax + Bu + Bd \tag{13}$$

$$x = \begin{bmatrix} x_1 \\ x_2 \end{bmatrix}, A = \begin{bmatrix} 0 & 1 \\ -a_1 & -a_2 \end{bmatrix}, B = \begin{bmatrix} 0 \\ b \end{bmatrix} \tag{14}$$

where:

$$\begin{aligned} a_1 &= \frac{1}{L_i C_i}, a_2 = \frac{\frac{1}{C_i} \left( \frac{I_{rg}}{V_{Tg}} + \frac{1}{R_{shg}} \right)}{\left( 1 + \frac{I_{rg}R_{sg}}{V_{Tg}} + \frac{R_{sg}}{R_{shg}} \right)}, b = \frac{\frac{1}{L_i C_i} \left( \frac{I_{rg}}{V_{Tg}} + \frac{1}{R_{shg}} \right)}{\left( 1 + \frac{I_{rg}R_{sg}}{V_{Tg}} + \frac{R_{sg}}{R_{shg}} \right)}, \\ d &= \frac{\frac{1}{L_i C_i} \left( \frac{I_{rg}}{V_{Tg}} + \frac{1}{R_{shg}} \right) I_{phg} + \ddot{I}_{phg}}{\left( 1 + \frac{I_{rg}R_{sg}}{V_{Tg}} + \frac{R_{sg}}{R_{shg}} \right)} \end{aligned} \tag{15}$$

Variable  $d$  is considered as uncertainty, due to unknown variables  $T, \dot{T}, \lambda,$  and  $\dot{\lambda}$ . Note that the pair  $(A, B)$  is controllable and that the matrix  $A$  is Hurwitz since  $a_1 > 0$  and  $a_2 > 0$ . Then, with the selection of any arbitrary symmetric positive definite matrix  $Q \in R^{2 \times 2}$ , one can find a symmetric positive definite matrix  $P \in R^{2 \times 2}$ , such that these matrixes satisfy the following Lyapunov equality equation [12]:

$$Q = -PA - A^T P \tag{16}$$

To have the maximum power of PGS, the output power, i.e.,  $P = VI$ , should be maximized and then, from Equation (9), we have:

$$\left(1 + \frac{I_{rg}R_{sg}}{V_{Tg}} + \frac{R_{sg}}{R_{shg}}\right) \frac{dI}{dV} + \left(\frac{I_{rg}}{V_{Tg}} + \frac{1}{R_{shg}}\right) = 0 \tag{17}$$

or:

$$\frac{dI}{dV} = -\frac{\left(\frac{I_{rg}}{V_{Tg}} + \frac{1}{R_{shg}}\right)}{\left(1 + \frac{I_{rg}R_{sg}}{V_{Tg}} + \frac{R_{sg}}{R_{shg}}\right)} = -C_{ia2} \tag{18}$$

or:

$$\frac{dP}{dV} = \frac{d(VI)}{dV} = I + \frac{dI}{dV} = x_1 - C_{ia2} = 0 \tag{19}$$

Therefore, the reference of the first state in Equation (13) can be written as  $x_{r1} = C_{ia2}$ . In this case, the sliding surface of dynamic SMC is defined as:

$$\begin{aligned} s &= \lambda_1(x_1 - x_{r1}) + \lambda_2(x_2 - \dot{x}_{r1}) + \lambda_3(\ddot{x}_2 - \ddot{x}_{r1}) \\ x_{r1} &= C_{ia2}, \dot{x}_{r1} = \ddot{x}_{r1} = 0 \end{aligned} \tag{20}$$

But, variable  $\dot{x}_2$  is unavailable due to the uncertainty in Equation (13). To solve this problem, a new DSO is designed. The following DSO is proposed for the system Equation (13):

$$\begin{cases} \dot{z}(t) = -z(t) + \mu_1(t) \\ \hat{\dot{x}}(t) = +z(t) + A\hat{x} + Bu + \mu_2(t) \end{cases} \tag{21}$$

where  $\mu_i : i = 1, 2$  are the observer inputs and the vector  $\hat{x}(t) = [\hat{x}_1, \hat{x}_2]^T$  is the estimation of the system states and  $z(t) = [z_1, z_2]^T \in \mathbb{R}^{2 \times 1}$  is the auxiliary vector signal and also  $|d| \leq D$ .

**Theorem 1.** *The observer error estimation  $e = x - \hat{x}$  converges to zero if the inputs of the observer are selected as follows:*

$$\begin{aligned} \mu_1 &= e \in \mathbb{R}^{2 \times 1} \\ \mu_2 &= P^{-1}(PBD + \text{sign}(e)) \in \mathbb{R}^{2 \times 1} \end{aligned} \tag{22}$$

**Proof of Theorem 1.** The error dynamic can be described as:

$$\dot{e}(t) = -z(t) + Ae + Bd - \mu_2(t) \tag{23}$$

Consider the following Lyapunov candidate function:

$$V(t) = \frac{1}{2}z(t)^T Pz(t) + \frac{1}{2}e(t)^T Pe(t) \tag{24}$$

then, we will have:

$$\dot{V} = \frac{1}{2}\dot{z}^T Pz + \frac{1}{2}z^T P\dot{z} + \frac{1}{2}\dot{e}^T Pe + \frac{1}{2}e^T P\dot{e} \tag{25}$$

Using the first part of the observer Equation (22) and the error dynamic Equation (24) one can write:

$$\begin{aligned} \dot{V} &= \frac{1}{2}(-z + \mu_1)^T Pz + \frac{1}{2}z^T P(-z + \mu_1) \\ &+ \frac{1}{2}(-z + Ae + Bd - \mu_2)^T Pe + \frac{1}{2}e^T P(-z + Ae + Bd - \mu_2) \end{aligned} \tag{26}$$

or:

$$\begin{aligned} \dot{V} = & -\frac{1}{2}z^T Pz + \frac{1}{2}\mu_1^T Pz - \frac{1}{2}z^T Pz + \frac{1}{2}z^T P\mu_1 \\ & -\frac{1}{2}z^T Pe + \frac{1}{2}e^T A^T Pe + \frac{1}{2}d B^T Pe - \frac{1}{2}\mu_2^T Pe \\ & -\frac{1}{2}e^T Pz + \frac{1}{2}e^T PAe + \frac{1}{2}d e^T PB - \frac{1}{2}e^T P\mu_2 \end{aligned} \tag{27}$$

Rearranging this leads to:

$$\dot{V} = -z^T Pz + z^T P\mu_1 - z^T Pe + \frac{1}{2}e^T (PA + A^T P)e + d e^T PB - e^T P\mu_2 \tag{28}$$

Using Equation (20) and the observer inputs Equation (22), it follows that:

$$\begin{aligned} \dot{V} = & -z^T Pz + z^T Pe - z^T Pe - \frac{1}{2}e^T Qe + d e^T PB - D e^T PB - e^T \text{sign}(e) \\ = & -z^T Pz - \frac{1}{2}e^T Qe + e^T PB(d - D) - e^T \text{sign}(e) \end{aligned} \tag{29}$$

Consider the following inequality:

$$\begin{aligned} -z^T Pz & \leq -\lambda_{\min}(P) \|z\|^2 \leq 0 \\ -e^T Qe & \leq -\lambda_{\min}(Q) \|e\|^2 \leq 0 \\ e^T PB & \leq |e| |P| |B| \leq |e| |P| \end{aligned} \tag{30}$$

where  $\lambda_{\min}$  is the minimum of eigen-value and therefore

$$\dot{V} \leq -\lambda_{\min}(P) \|z\|^2 - \frac{1}{2}\lambda_{\min}(Q) \|e\|^2 + |e| |P| (|d| - D) - \sum_{i=1}^2 |e_i| \tag{31}$$

Inequality  $|d| \leq D$  results  $\dot{V} \leq 0$  and consequently the signal  $z$  and the error dynamic  $e$  converge to zero. □

#### 4. Sliding Mode Control Design

To have the chattering-less duty cycle, a new proposed dynamic SMC is constructed and then conventional SMC is designed in order to compare it with the dynamic SMC. The validity of the comparison is comprehensive due to the use of the same DSO Equation (21) in both approaches. According to the observer Equation (21), one can conclude the following equations.

$$\dot{\hat{x}}_1 = z_1 + \hat{x}_2 + C_1\mu_2, C_1 = [1, 0] \tag{32}$$

$$\dot{\hat{x}}_2 = z_2 - a_1\hat{x}_1 - a_2\hat{x}_2 + bu + C_2\mu_2, C_2 = [0, 1] \tag{33}$$

$$\ddot{\hat{x}}_2 = \dot{z}_2 - a_1\dot{\hat{x}}_1 - a_2\dot{\hat{x}}_2 + b\dot{u} = -z_2 + C_2\mu_1 - a_1\dot{\hat{x}}_1 - a_2\dot{\hat{x}}_2 + b\dot{u} \tag{34}$$

The proof of chattering-less closed loop stability of dynamic SMC controller is presented as follows:

**Theorem 2.** *The following signal causes the sliding surface in Equation (20) to reach zero in finite time.*

$$\dot{u} = -\frac{\lambda_1 x_2 + \lambda_2 \dot{x}_2 + \lambda_3 (-z_2 + C_2\mu_1 - a_1\dot{\hat{x}}_1 - a_2\dot{\hat{x}}_2) + \eta_1 s + \eta_2 \text{sign}(s)}{b\lambda_3} \tag{35}$$

**Proof of Theorem 2.** From Equations (32)–(34) one can write:

$$\begin{aligned}\dot{s} &= \lambda_1 \dot{x}_1 + \lambda_2 \dot{x}_2 + \lambda_3 \ddot{x}_2 = \lambda_1 x_2 + \lambda_2 \dot{x}_2 + \lambda_3 \ddot{x}_2 \\ &= \lambda_1 x_2 + \lambda_2 \dot{x}_2 + \lambda_3 (-z_2 + C_2 \mu_1 - a_1 \dot{x}_1 - a_2 \dot{x}_2 + b \dot{u})\end{aligned}\quad (36)$$

Substituting Equation (35) into Equation (36) results in:

$$\dot{s} = -\eta_1 s - \eta_2 \text{sign}(s)\quad (37)$$

Using the Lyapunov function  $V = 0.5 s^2$ , then:

$$\dot{V} = \dot{s}s = s(-\eta_1 s - \eta_2 \text{sign}(s)) = -\eta_1 s^2 - \eta_2 |s| \leq -\eta_2 |s|\quad (38)$$

Suppose  $t$  would be the finite reaching time to the sliding surface, then one can conclude that  $t \leq \frac{|s(0)|}{\eta_2}$  [13].  $\square$

Now, in the following theorem closed loop stability of conventional SMC controller is proved.

**Theorem 3.** Consider the following sliding surface:

$$\begin{aligned}s &= \lambda_1 (x_1 - x_{r1}) + \lambda_2 (x_2 - \dot{x}_{r1}) \\ x_{r1} &= C_1 a_2, \dot{x}_{r1} = 0\end{aligned}\quad (39)$$

Then, the following signal causes the sliding surface in Equation (39) to reach zero in finite time.

$$u = -\frac{\lambda_1 x_2 + \lambda_2 (z_2 - a_1 \dot{x}_1 - a_2 \dot{x}_2 + C_2 \mu_2) + \eta_1 s + \eta_2 \text{sign}(s)}{b \lambda_2}\quad (40)$$

**Proof of Theorem 3.** From Equation (33) one can write:

$$\dot{s} = \lambda_1 \dot{x}_1 + \lambda_2 \dot{x}_2 = \lambda_1 x_2 + \lambda_2 \dot{x}_2 = \lambda_1 x_2 + \lambda_2 (z_2 - a_1 \dot{x}_1 - a_2 \dot{x}_2 + b u + C_2 \mu_2)\quad (41)$$

Substituting Equation (40) into Equation (41) results in:

$$\dot{s} = -\eta_1 s - \eta_2 \text{sign}(s)\quad (42)$$

Using the Lyapunov function  $V = 0.5 s^2$ , then:

$$\dot{V} = \dot{s}s = s(-\eta_1 s - \eta_2 \text{sign}(s)) = -\eta_1 s^2 - \eta_2 |s| \leq -\eta_2 |s|\quad (43)$$

Suppose  $t$  would be the finite reaching time to the sliding surface, then one can conclude that  $t \leq \frac{|s(0)|}{\eta_2}$  [13].  $\square$

**Remark 1.** The coefficients  $\lambda_i$  in sliding surfaces Equations (20) and (39) are selected such that the zero dynamics of surface will be stable. In this case  $x_1$  tracks its desired value, i.e.,  $x_{r1}$ .

## 5. Simulations Presentation

The solar panel used in this research is TE500CR [44] and hence the parameters of the PV cells are as in Table 1 and also the parameters of the converter are denoted in Table 2.

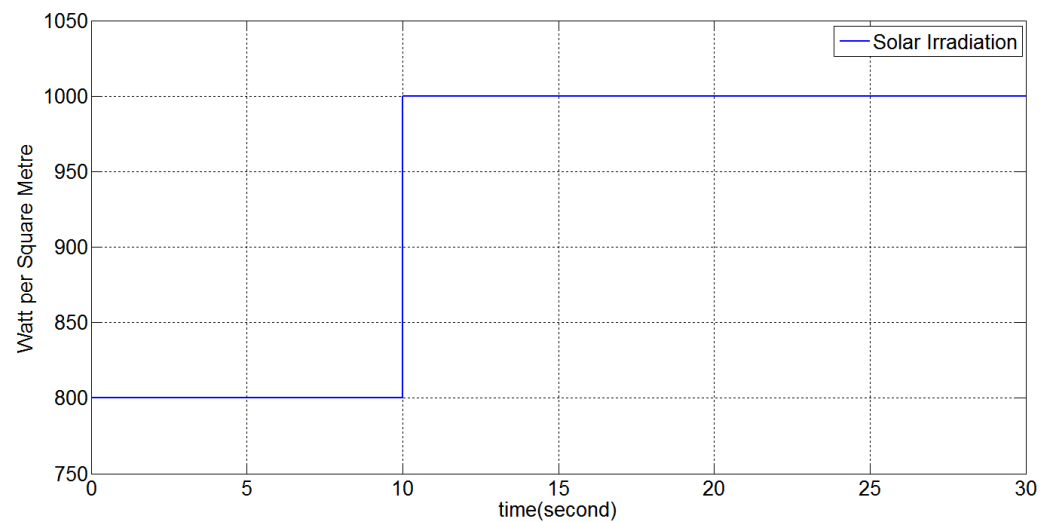
**Table 1.** The parameters of the PV cells.

Parameter	Value	Unit
$I_r$	4.842	$\mu\text{A}$
$I_{sc}$	3.45	A
$R_s$	0.1124	$\Omega$
$R_{sh}$	6500	$\Omega$
$T_r$	298.15	$^{\circ}\text{K}$

**Table 2.** The parameters of the converter.

Parameter	Value	Unit
$V_c$	400	V
$I_c$	12.5	A
$L_i$	3.5	mH
$C_i$	4700	$\mu\text{F}$
$C_o$	470	$\mu\text{F}$

In addition,  $N_p = 20$ ,  $N_s = 20$ , and all the observer initial values are set to zero, i.e.,  $\hat{x}(0) = [0, 0]^T$  and  $z(0) = [0, 0]^T$ . For a reliable comparison, two simulations are carried out using dynamic SMC and conventional SMC, both based on the same DSO observer. Both simulations are carried out with Matlab using a step size of 0.001. The solar irradiation and the cell temperature are shown in Figures 4 and 5. The solar irradiation has increased from  $\lambda = 800 \text{ W/m}^2$  to  $\lambda = 1000 \text{ W/m}^2$  at time 10 s, and the temperature has increased from  $T = 298.15 \text{ }^{\circ}\text{K}$  to  $T = 325 \text{ }^{\circ}\text{K}$  at time 20 s.

**Figure 4.** Variations of solar irradiation.



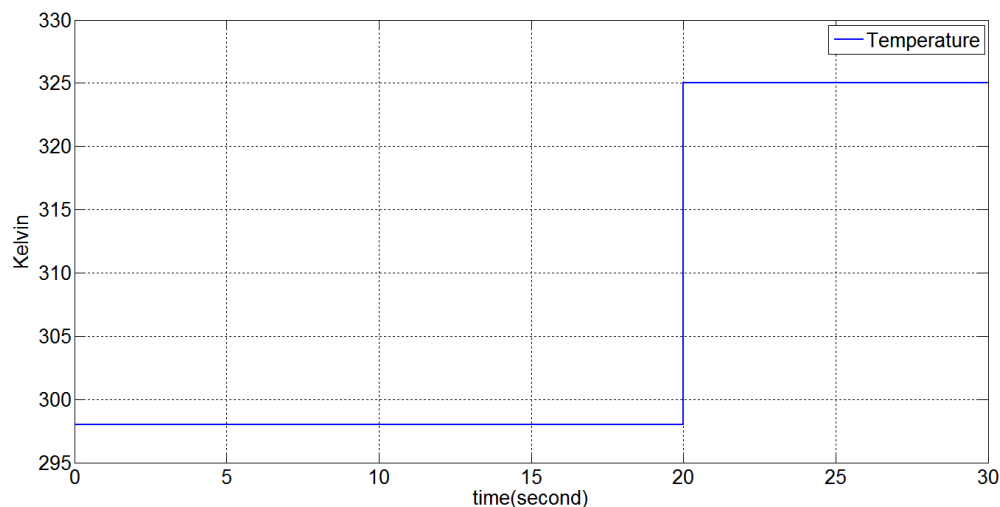


Figure 5. Variations in temperature.

**Remark 2.** For calculation of input control duty cycle, we first calculate variables in Equations (32)–(34) using the observer Equation (21). Then input can be obtained from Equation (35) for dynamic SMC and from Equation (40) for conventional SMC.

**Example 1.** The dynamic SMC proposed approach.

The sliding surface coefficients are selected as  $\lambda_1 = 5$ ,  $\lambda_2 = 1$ , and  $\lambda_3 = 0.1$ ; in addition, we choose  $\eta_1 = 5$  and  $\eta_2 = 2$ . Moreover, to calculate the input control signal from the Equation (35) we need an initial value selected as  $u(0) = 0$ . The results are presented in Figures 6–9. Figure 6 shows the output current of PGS, which is tracked the  $x_{r1} = C_1 a_2$  and Figures 7 and 8 present the output voltage of PGS and the smooth duty cycle of the converter. We can see that when the output voltage of PGS increases, the duty cycle decreases. This causes the output voltage of the converter to remain fixed at  $V_c = 400$ . The convergence of sliding surface to zero is shown in Figure 9. We can see that all the figures in this example are without chattering.

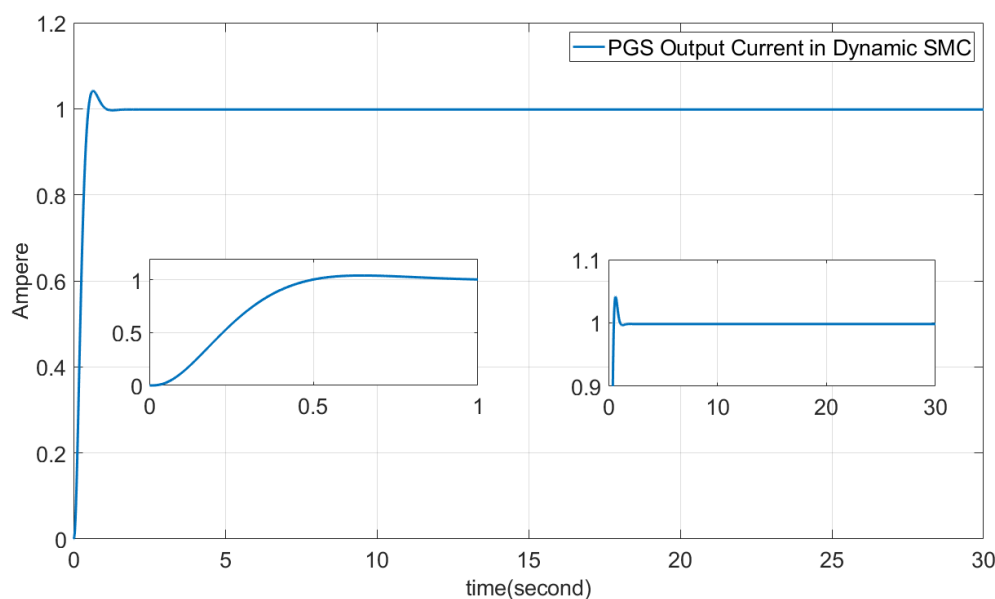


Figure 6. PGS output current in dynamic SMC.

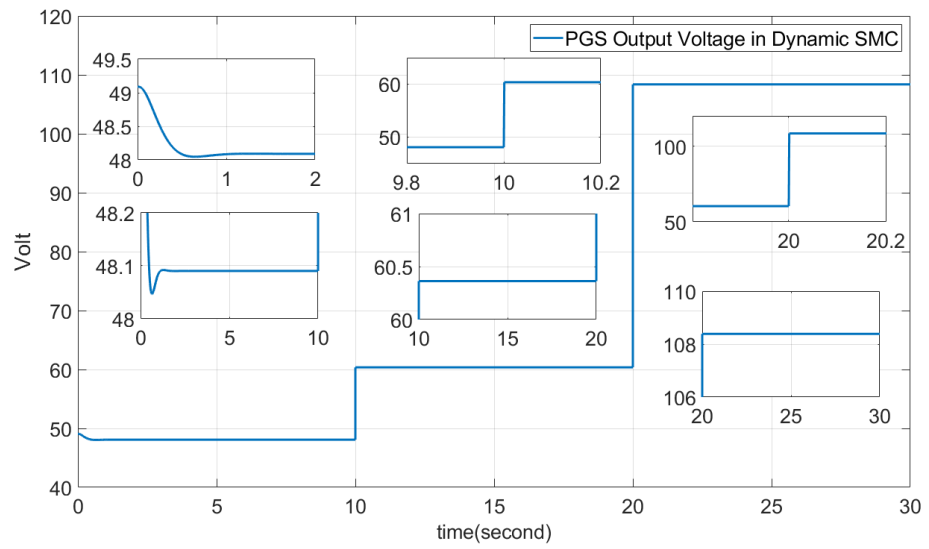


Figure 7. PGS output voltage in dynamic SMC.

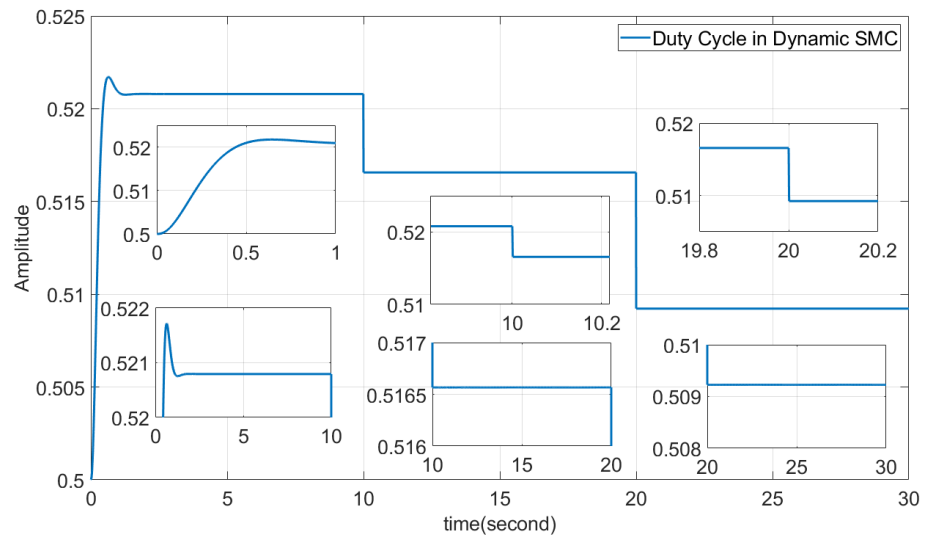


Figure 8. Duty cycle of the converter in dynamic SMC.

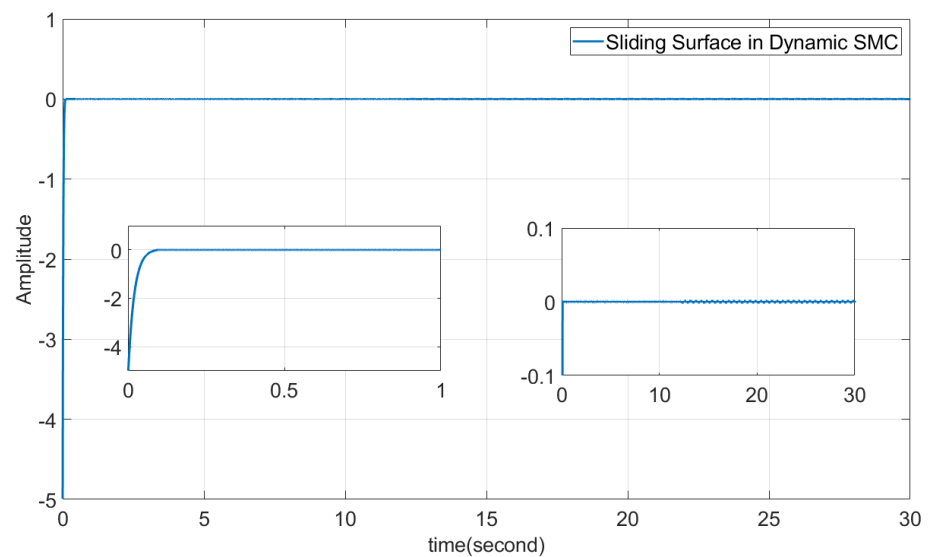
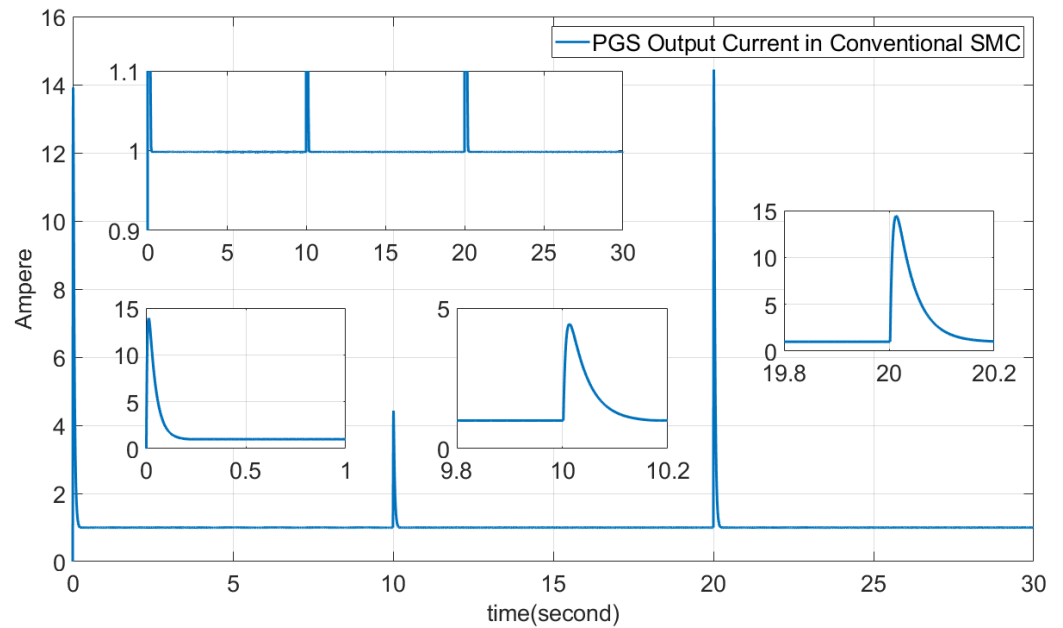


Figure 9. Sliding surface in dynamic SMC.

**Example 2.** *The conventional SMC.*

In this example conventional SMC is simulated with the same parameters of example 1; i.e., the sliding surface coefficients Equation (39) are selected as  $\lambda_1 = 5$  and 1. In addition, we choose  $\eta_1 = 5$  and  $\eta_2 = 2$ . The results are presented in Figures 10–13. Figure 10 shows the output current of PGS, which is tracked as  $x_{r1} = C_{i2}$ , and Figures 11 and 12 present the output voltage of PGS and the duty cycle of the converter. The convergence of sliding surface to zero is shown in Figure 13. The effect of chattering can be seen in these figures.



**Figure 10.** PGS output current in conventional SMC.

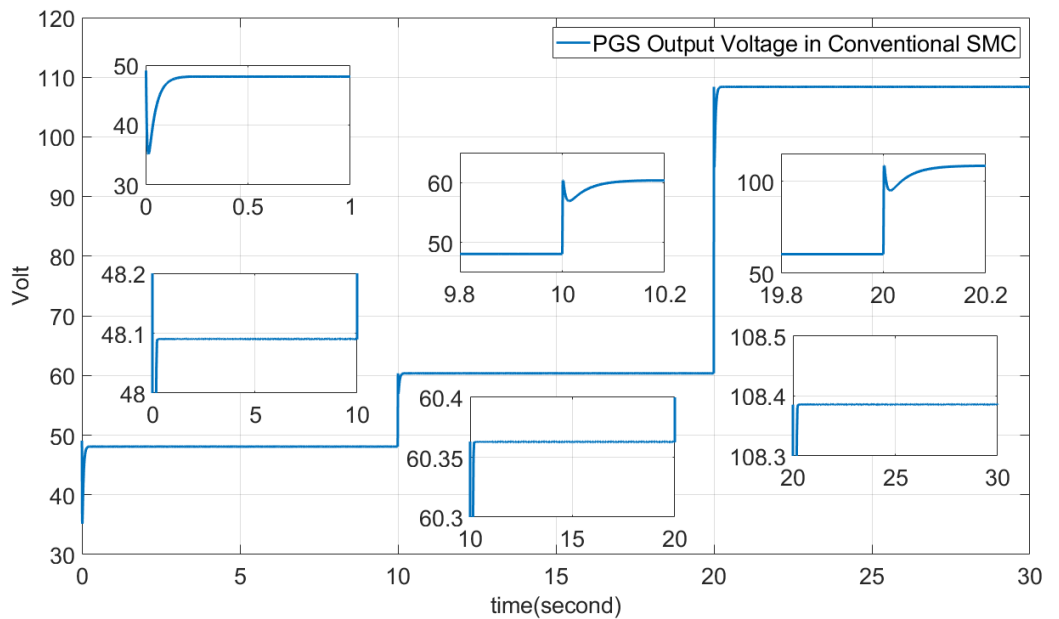


**Figure 11.** PGS output voltage in conventional SMC.

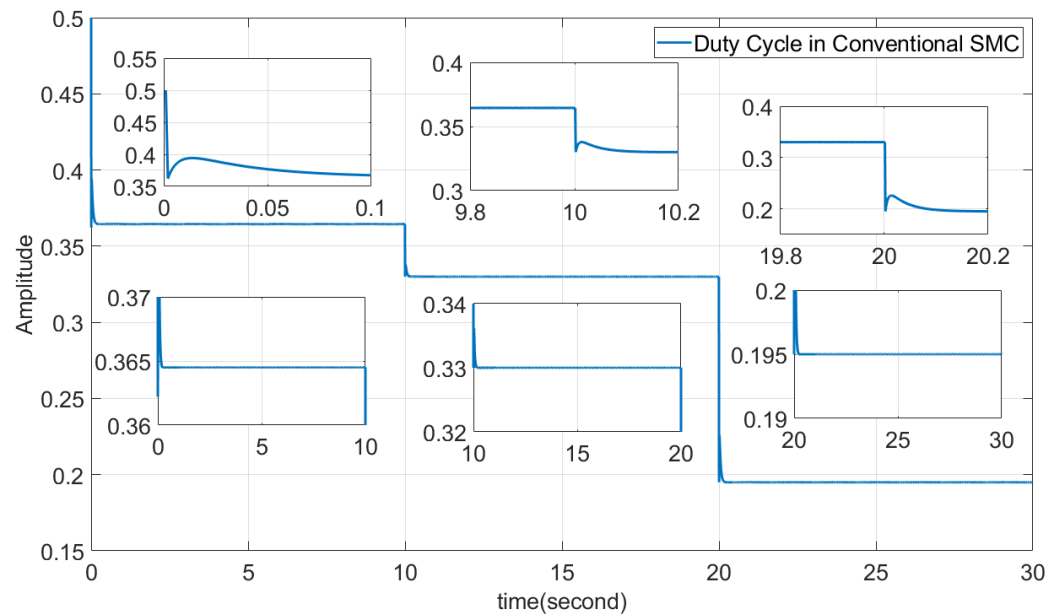


Figure 12. Duty cycle of the converter in conventional SMC.

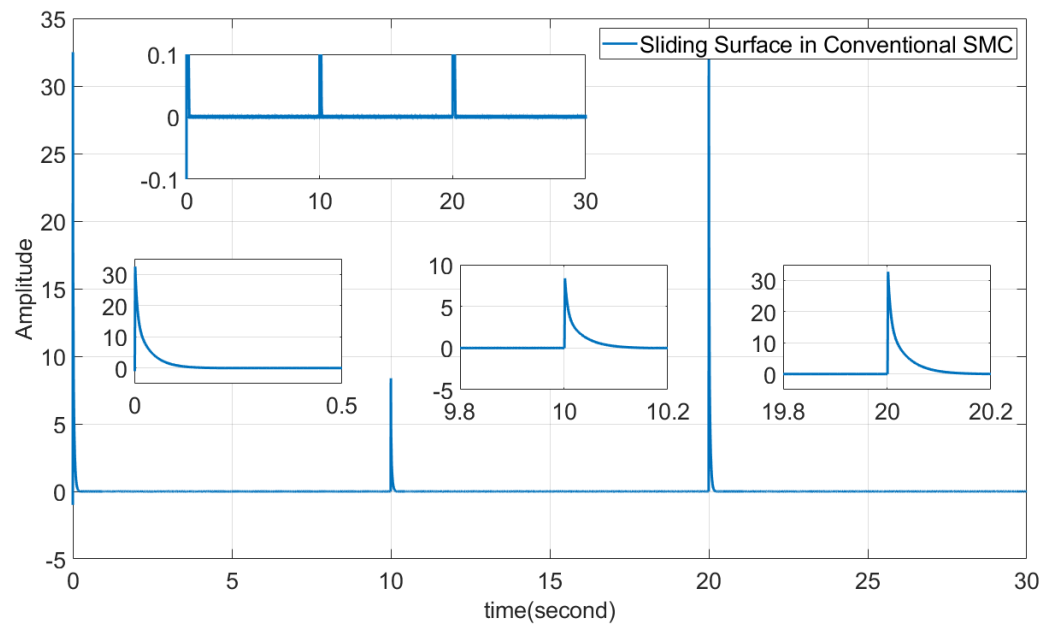


Figure 13. Sliding surface in conventional SMC.

**Comparison and Discussion:** From comparison of these figures one can see the good performance of the proposed DSO. Nevertheless, in the viewpoint of the controller design, the dynamic SMC has better performance, which can be seen from comparison of the figures. Moreover, dynamic SMC has better performance in chattering suppression than conventional SMC. The chattering effect can be observed from Figure 13. Note that this chattering can reduce the effectiveness and efficiency of the controller and furthermore can damage the electrical parts. As the simulations results show, the steady state of the two approaches is zero. This can be seen from Figures 9 and 13, where the sliding surfaces converge to zero in finite time. Finally, the simple design of dynamic SMC with respect to conventional SMC can be observed.

## 6. Conclusions

In this paper, a new approach is presented for smooth duty cycle regulation of a converter, which is placed after the photovoltaic generator system (PGS). It has been shown that by suitable selection of the duty cycle of the converter, the maximum power point tracking (MPPT) of PGS is achieved. The augmented system, i.e., the PGS and the converter, has some uncertainties, however. To overcome the uncertainty and have a smooth duty cycle, we propose a new robust chattering-less controller approach, which is based on a dynamic sliding mode control (Dynamic SMC). To implement the dynamic SMC, a new structure of the dual sliding observer (DSO) is constructed. Then a comparison is carried out by the conventional sliding mode control (Conventional SMC) with the same DSO and similar parameters. This comparison shows that chattering presents in the conventional SMC but it is eliminated in the dynamic SMC. Moreover, the simple concept and realization of dynamic SMC is evident. Closed-loop stability is provided using Lyapunov theory.

**Author Contributions:** A.K.-M.: analysis, writing original draft and preparation; O.B.: conceptualization, review, and editing. All authors have read and agreed to the published version of the manuscript.

**Funding:** This study received no external funding.

**Institutional Review Board Statement:** Not applicable.

**Informed Consent Statement:** Not applicable.

**Data Availability Statement:** Not applicable.

**Acknowledgments:** The authors wish to express their gratitude to the Basque Government, through the project EKOHEGAZ (ELKARTEK KK-2021/00092), to the Diputación Foral de Álava (DFA), through the project CONAVANTER, and to the UPV/EHU, through the project GIU20/063, for supporting this work.

**Conflicts of Interest:** The authors declare no conflict of interest.

## References

1. De Battista, H.; Mantz, R.J. Variable structure control of a photovoltaic energy converter. *IEE Proc. Control Theory Appl.* **2002**, *149*, 303–310. [[CrossRef](#)]
2. Song, Y.D.; Dhinakaran, B.; Bao, X.Y. Variable speed control of wind turbines using nonlinear and adaptive algorithms. *Wind Eng. Ind. Aerodyn.* **2000**, *85*, 293–308. [[CrossRef](#)]
3. Barambones, O.; Cortajarena, J.A.; Calvo, I.; Gonzalez de Durana, J.M.; Alkorta, P.; Karami-Mollae, A. Variable speed wind turbine control scheme using a robust wind torque estimation. *Renew. Energy* **2019**, *133*, 354–366. [[CrossRef](#)]
4. Karami, N.; Moubayed, N.; Outbib, R. General review and classification of different MPPT techniques. *Renew. Sustain. Energy Rev.* **2017**, *68*, 1–18. [[CrossRef](#)]
5. Adhikari, S.; Li, F.; Li, H. P-Q and P-V control of photovoltaic generators in distribution systems. *IEEE Trans. Smart Grid* **2015**, *6*, 2929–2941. [[CrossRef](#)]
6. El Khazane, J.; El Tissir, H. Achievement of MPPT by finite time convergence sliding mode control for photovoltaic pumping system. *Sol. Energy* **2018**, *166*, 13–20. [[CrossRef](#)]
7. Miqoi, S.; El Ougli, A.; Tidhaf, B. Adaptive fuzzy sliding mode based MPPT controller for a photovoltaic water pumping system. *Int. J. Power Electron. Drive Syst.* **2019**, *10*, 414–422. [[CrossRef](#)]
8. Dounis, A.I.; Kofinas, P.; Papadakis, G.; Alafodimos, C. A direct adaptive neural control for maximum power point tracking of photovoltaic system. *Sol. Energy* **2015**, *115*, 145–165. [[CrossRef](#)]
9. Na, W.; Chen, P.; Kim, J. An improvement of a fuzzy logic-controlled maximum power point tracking algorithm for photovoltaic applications. *Appl. Sci.* **2017**, *7*, 326. [[CrossRef](#)]
10. Nabipour, M.; Razaz, M.; Seifossadat, S.; Mortazavi, S. A new MPPT scheme based on a novel fuzzy approach. *Renew. Sustain. Energy Rev.* **2017**, *74*, 1147–1169. [[CrossRef](#)]
11. Wang, C.-C.; Jose, O.L.J.A.; Su, P.K.; Tolentino, L.K.S.; Sangalang, R.G.B.; Velasco, J.S.; Lee, T.J. An adaptive constant current and voltage mode P&O-based maximum power point tracking controller IC using 0.5- $\mu\text{m}$  HV CMOS. *Microelectron. J.* **2021**, *118*, 105295.
12. Slotine, J.J.E.; Li, W. *Applied Nonlinear Control*; Prentice Hall: Englewood Cliffs, NJ, USA, 1991.
13. Karami-Mollae, A.; Pariz, N.; Shanechi, H.M. Position control of servomotors using neural dynamic sliding mode. *J. Dyn. Syst. Meas. Control* **2011**, *133*, 141–150. [[CrossRef](#)]

14. Perruquetti, W.; Barbot, J.P. *Sliding Mode Control in Engineering*; Marcel Dekker: New York, NY, USA, 2002.
15. Chu, C.-C.; Chen, C.-L. Robust maximum power point tracking method for photovoltaic cells: A sliding mode control approach. *Sol. Energy* **2009**, *83*, 1370–1378. [[CrossRef](#)]
16. Bianconi, E.; Calvente, J.; Giral, R.; Mamarelis, E.; Petrone, G.; Ramos-Paja, C.A.; Spagnuolo, G.; Vitelli, M. Perturb and Observe MPPT algorithm with a current controller based on the sliding mode. *Int. J. Electr. Power Energy Syst.* **2013**, *44*, 346–356. [[CrossRef](#)]
17. Yatimi, H.; Aroudam, E. Assessment and control of a photovoltaic energy storage system based on the robust sliding mode MPPT controller. *Sol. Energy* **2016**, *139*, 557–568. [[CrossRef](#)]
18. Cortajarena, J.A.; Barambones, O.; Alkorta, P.; De Marcos, J. Sliding mode control of grid-tied single-phase inverter in a photovoltaic MPPT application. *Sol. Energy* **2017**, *155*, 793–804. [[CrossRef](#)]
19. Mojallizadeh, M.R.; Badamchizadeh, M.A. Second-order fuzzy sliding-mode control of photovoltaic power generation systems. *Sol. Energy* **2017**, *149*, 332–340. [[CrossRef](#)]
20. Kumar, N.; Saha, T.K.; Dey, J. Sliding mode control, implementation and performance analysis of standalone PV fed dual inverter. *Sol. Energy* **2017**, *155*, 1178–1187. [[CrossRef](#)]
21. Kchaou, A.; Naamane, A.; Koubaa, Y.; M'sirdi, N. Second order sliding mode-based MPPT control for photovoltaic applications. *Sol. Energy* **2017**, *155*, 758–769. [[CrossRef](#)]
22. Chihi, A.; Azza, H.B.; Jemli, M.; Sellami, A. Nonlinear integral sliding mode control design of photovoltaic pumping system: Real time implementation. *ISA Trans.* **2017**, *70*, 475–485. [[CrossRef](#)]
23. Lee, H.; Utkin, V.-I. Chattering suppression methods in sliding mode control systems. *Annu. Rev. Control* **2007**, *31*, 179–188. [[CrossRef](#)]
24. Fuh, C.-C. Variable-thickness boundary layers for sliding mode control. *J. Mar. Sci. Technol.* **2008**, *16*, 288–294. [[CrossRef](#)]
25. Chen, H.-M.; Renn, J.-C.; Su, J.-P. Sliding mode control with varying boundary layers for an electro-hydraulic position servo system. *Int. J. Adv. Manuf. Technol.* **2005**, *26*, 117–123. [[CrossRef](#)]
26. Zhang, X. Sliding mode-like fuzzy logic control with adaptive boundary layer for multiple-variable discrete. *J. Intell. Syst.* **2016**, *25*, 209–220. [[CrossRef](#)]
27. Allamehzadeh, H.; Cheung, J.Y. Optimal fuzzy sliding mode control with adaptive boundary layer. *WSEAS Trans. Syst.* **2004**, *3*, 1887–1892.
28. Cucuzzella, M.; Incremona, G.P.; Ferrara, A. Design of robust higher order sliding mode control for micro grids. *IEEE J. Emerg. Sel. Top. Circuits Syst.* **2015**, *5*, 393–401. [[CrossRef](#)]
29. Nonaka, R.; Yamashita, Y.; Tsubakino, D. General scheme for design of higher-order sliding-mode controller. In Proceedings of the American Control Conference (ACC), Chicago, IL, USA, 1–3 July 2015; pp. 5176–5181.
30. Koshkouei, A.J.; Burnham, K.J.; Zinober, A.S. Dynamic sliding mode control design. *IEE Proc. Control Theory Appl.* **2005**, *152*, 392–396. [[CrossRef](#)]
31. Chen, M.-S.; Chen, C.-H.; Yang, F.-Y. An LTR-observer based dynamic sliding mode control for chattering reduction. *Automatica* **2007**, *43*, 1111–1116. [[CrossRef](#)]
32. Levant, A. Sliding order and sliding accuracy in sliding mode control. *Int. J. Control* **1993**, *58*, 1247–1263. [[CrossRef](#)]
33. Levant, A. Homogeneity approach to high-order sliding mode design. *Automatica* **2005**, *41*, 823–830. [[CrossRef](#)]
34. Plestan, F.; Glumineau, A.; Laghrouche, S. A new algorithm for high-order sliding mode control. *Int. J. Robust Nonlinear Control* **2008**, *18*, 441–453. [[CrossRef](#)]
35. Shtessel, Y.B.; Fridman, L.; Zinober, A. Higher order sliding modes. *Int. J. Robust Nonlinear Control* **2008**, *18*, 381–384. [[CrossRef](#)]
36. Yang, Y.; Qin, S.; Jiang, P. A modified super-twisting sliding mode control with inner feedback and adaptive gain schedule. *Int. J. Adapt. Control Signal Process.* **2017**, *31*, 398–416. [[CrossRef](#)]
37. Butt, Q.R.; Bhatti, A.I.; Mufti, M.R.; Rizvi, M.A.; Awan, I. Modeling and online parameter estimation of intake manifold in gasoline engines using sliding mode observer. *Simul. Model. Pract. Theory* **2013**, *32*, 138–154. [[CrossRef](#)]
38. Davila, J.; Fridman, L.; Levant, A. Second-order sliding mode observer for mechanical systems. *IEEE Trans. Autom. Control* **2005**, *50*, 1785–1789. [[CrossRef](#)]
39. Liu, Y.-T.; Kung, T.-T.; Chang, K.-M.; Chen, S.-Y. Observer-based adaptive sliding mode control for pneumatic servo system. *Precis. Eng.* **2013**, *37*, 522–530. [[CrossRef](#)]
40. Xia, Y.; Zhu, Z.; Fu, M. Back-stepping sliding mode control for missile systems based on an extended state observer. *IET Control Theory Appl.* **2011**, *5*, 93–102. [[CrossRef](#)]
41. Fuyang, C.; Lei, W.; Zhang, K.; Tao, G.; Jiang, B. A novel nonlinear resilient control for a quadrotor UAV via backstepping control and nonlinear disturbance observer. *Nonlinear Dyn.* **2016**, *85*, 1281–1295.
42. Xiong, Y.; Saif, M. Sliding mode observer for nonlinear uncertain systems. *IEEE Trans. Autom. Control* **2001**, *46*, 2012–2017. [[CrossRef](#)]
43. Benchaib, A.; Rachid, A.; Audrezet, E.; Tadjine, M. Real time sliding-mode observer and control of an induction motor. *IEEE Trans. Ind. Electron.* **1999**, *46*, 128–138. [[CrossRef](#)]
44. Akbaba, M. Optimum matching parameters of an MPPT unit based for a PVG-powered water pumping system for maximum power transfer. *Int. J. Energy Resour.* **2006**, *30*, 395409.